Joint optimization of coding mask and scan positions for compressive single sensor imaging

van der Meulen, P.Q.; Kruizinga, P.; Bosch, J.G.; Leus, G.J.T.

DOI
10.1109/ULTSYM.2018.8579728

Publication date
2018

Document Version
Final published version

Published in
2018 IEEE International Ultrasonics Symposium (IUS)

Joint optimization of coding mask and scan positions for compressive single sensor imaging

Pim van der Meulen*, Pieter Kruizinga†‡, Johannes G. Bosch‡, Geert Leus*
*Delft University of Technology, Circuits and Systems, Delft, Netherlands
†Erasmus Medical Center, Department of Neuroscience, Rotterdam, Netherlands
‡Erasmus Medical Center, Department of Biomedical Engineering, Rotterdam, Netherlands

***Abstract*—We study the optimal design of an aperture coding mask, and the optimal sensing positions of a single ultrasound sensor with a scanning configuration. In previous works, we have shown that 3D ultrasound imaging is possible using a randomly shaped coding mask with randomly chosen sensing positions. Here we propose an optimization algorithm for the joint design of the coding mask and the sensing positions. We first define a linear measurement model and parameterize it with respect to the mask shape. To optimize the shape of the mask, we use a greedy descent algorithm to minimize the imaging MSE, assuming a Wiener estimate is used for image reconstruction. To optimize the sensing positions, we pre-define a set of such sensing positions by gridding the measurement plane, and regard each sensing position as a virtual sensor candidate. We then use a greedy sensor selection algorithm to find a good selection of sensing positions. To jointly optimize for both the mask and the sensing positions, we alternatingly optimize between them, keeping either the mask shape or the sensing positions fixed. Using simulations we show that the joint optimization results in better imaging performance than optimizing for the mask or the sensing positions alone, or using a completely random design.**

I. Introduction

In recent years there has been a growing interest in reducing the amount of measurement data from ultrasound arrays while retaining image quality. The theory of Compressive Sensing ([1]–[4]) provides us with tools for undersampling measurement data below the Nyquist limit, provided that the signal under recovery has a sparse representation in a known domain. This resulted in a large number of studies in the medical ultrasound imaging community, typically using random subsampling in space and/or time, or using random compression schemes ([5]–[10], amongst others). Recently, we demonstrated a single sensor ultrasound imaging system by equipping the sensor with a *coding mask* [11], that does not rely on sparsity, but uses straight-forward ℓ_2 regularization for imaging. The basic principle is as follows. Consider a circular single ultrasound sensor, its flat surface aligned to a reference plane, without a coding mask. Ultrasound reflectors at the same *range*, and the same altitudinal angle with respect to the reference plane have the same pulse-echo signal shape across all the azimuth, making them unresolvable. If, on the other hand, a irregular material is placed in between the ultrasound sensor and the imaging object, this will distort the ultrasound waves in a direction-dependent manner. As a result, two scatterers at the same range will reflect different ultrasound wavefields to the sensor (for a more detailed review, see [11]). These scatterers can then be resolved based on the difference of the measured waveforms.

As an extension of this idea, we recently showed a single sensor with a coding mask that is translated in space [12]. By moving the sensor to a different position, more information about the image target is obtained. These kind of imaging systems can be used in a catheter-based imaging scenario, where the inside of the veins, arteries, or the heart is imaged to assist in minimally invasive surgery. Since a single sensor is employed instead of an array, a very small amount of data is transferred to an imaging unit outside the patient, resulting in smaller devices and less data cables.

In our works so far, we have only considered using a randomly shaped coding mask, and in [12] we also used randomly selected sensing positions. However, it is not known how optimal a random setup performs, or whether a performance increase is possible using a deterministic design. In this paper, we propose a greedy optimization algorithm to find a good mask shape, as well as a good set of sensing positions. Since this greedy algorithm is sub-optimal, it is not guaranteed to find the true optimum, but our simulation results show a significant performance increase compared to randomized sensing configurations.

II. Methods

Denoting vectors in lowercase bold, and matrices in uppercase bold, we assume the following linear model

$$\mathbf{y}_k = \mathbf{A}_k\mathbf{x} + \mathbf{n}_k, \tag{1}$$

where $\mathbf{y}_k \in \mathbb{C}^N$ is the pulse-echo measurement vector consisting of frequency domain samples for measurement position k. The vector $\mathbf{x} \in \mathbb{R}^M$ is a real-valued vector containing the image values of each pixel in the ROI, and $\mathbf{A}_k \in \mathbb{C}^{M\times N}$ describes the relation between $\mathbf{y}_k$ and $\mathbf{x}$, consisting of Green's functions for each image pixel. The vector $\mathbf{n}_k \in \mathbb{C}^N$ represents additive measurement noise, which we assume is white, independent and identically distributed, and Gaussian: $\mathbf{n}_k \sim \mathcal{N}(\mathbf{0}, \sigma_n^2\mathbf{I})$, where σ_n^2 is the noise variance.

If K measurements are taken by scanning the ultrasound probe, the measurements can be stacked to obtain a larger system of equations:

$$\begin{bmatrix}\mathbf{y}_1^\mathsf{T} & \mathbf{y}_2^\mathsf{T} & \dots & \mathbf{y}_K^\mathsf{T}\end{bmatrix}^\mathsf{T} = \begin{bmatrix}\mathbf{A}_1^\mathsf{T} & \mathbf{A}_2^\mathsf{T} & \dots & \mathbf{A}_K{}^\mathsf{T}\end{bmatrix}^\mathsf{T}\mathbf{x} + \mathbf{n}, \tag{2}$$

which we will denote shortly as $\mathbf{y} = \mathbf{A}\mathbf{x} + \mathbf{n}$. In this paper, we assume that an estimate of $\mathbf{x}$ is obtained by using a Wiener estimator. Since $\mathbf{A}$ describes the difficulty of the imaging

This work is part of the ASPIRE project (project 14926 within the STW OTP programme), and the PUMA project (project 13154 within the STW OTP programme), which are financed by the Netherlands Organisation for Scientific Research (NWO).

problem, we will use it to find a good mask and set of sensing positions. Therefore, we will parameterize the measurement matrix $\mathbf{A}$ by the mask shape parameter $\mathbf{w}$ and the sensing positions parameter $\mathbf{v}$, denoted as $\mathbf{A}(\mathbf{v}, \mathbf{w})$.

To find a good $\mathbf{v}$ and $\mathbf{w}$, we will use the estimation error covariance matrix given by

$$\mathbf{C}_\epsilon = (\mathbf{C}_x^{-1} + 1/\sigma_n^2 \mathbf{A}(\mathbf{v}, \mathbf{w})^\mathsf{H} \mathbf{A}(\mathbf{v}, \mathbf{w}))^{-1}, \tag{3}$$

where $\mathbf{C}_x$ is the covariance matrix of $\mathbf{x}$, and we assume in this work that $\mathbf{C}_x = \mathbf{I}$. The imaging mean squared error (MSE) is simply the sum of the diagonal entries of $\mathbf{C}_\epsilon$:

$$\text{MSE} = \text{trace}(\mathbf{C}_\epsilon) \tag{4}$$

Hence, we would ideally minimize this MSE with respect to $\mathbf{v}$ and $\mathbf{w}$. This is, however, a non-convex problem, so in the next section we present two algorithms to find sub-optimal solutions.

A. Optimizing for sensing positions

We first define a grid of candidate sensing positions. If the mask is fixed, each of these points can be seen as a virtual sensor, and we can easily pre-compute the $\mathbf{A}_k$ for each of these sensor candidates. If the v-th element of $\mathbf{v} \in \{0,1\}^V$ indicates whether the sensing position v (with corresponding sensing matrix $\mathbf{A}_v(\mathbf{w})$ is used or not, the matrix $\mathbf{C}_\epsilon^{-1}$ is then expressed as

$$\mathbf{C}_\epsilon^{-1} = \mathbf{C}_x^{-1} + 1/\sigma_n^2 \sum_{v=1}^{V} [\mathbf{v}]_v \mathbf{A}_v(\mathbf{w})^\mathsf{H} \mathbf{A}_v(\mathbf{w}). \tag{5}$$

Of course, if we want to select K sensing positions, then only K components of $\mathbf{v}$ should be one, and all others zero. This is a well known *sensor-selection* problem, which can be solved using convex optimization techniques [13], [14]. An alternative approach in sensor-selection literature is to use a greedy optimization algorithm [15]–[17], which has known worst-case bounds on the optimality of the solution if the considered cost-function is sub-modular [18]. Inspired by such works, we will use the same greedy algorithm to find a good set of sensing functions. Although the MSE (4) is not a sub-modular function with respect to $\mathbf{v}$, there are studies that show the MSE cost-function can be solved near-optimally using greedy selection (e.g. [19]). The algorithm is shown in Alg. 1.

Algorithm 1 Greedy position selection algorithm

1: Input: set of sensor candidates $\mathcal{A}$
2: Output: measurement matrix of selected positions $\hat{\mathbf{A}}$
3: Initialize $\hat{\mathbf{A}} = [\,]$
4: **for** $k = 1, 2, \ldots, K$ **do**
5: $\quad \hat{\mathbf{A}}_k = \arg\min_{\mathbf{A} \in \mathcal{A}} \text{MSE}(\left[\hat{\mathbf{A}}^\mathsf{T} \ \mathbf{A}^\mathsf{T}\right]^\mathsf{T})$
6: $\quad \hat{\mathbf{A}} = \left[\hat{\mathbf{A}}^\mathsf{T} \ \hat{\mathbf{A}}_k^\mathsf{T}\right]^\mathsf{T}$
7: $\quad \mathcal{A} = \mathcal{A} \setminus \mathbf{A}_k$
8: **end for**

B. Optimizing for the mask shape

If the sensing positions $\mathbf{v}$ are known, we use the mask optimization algorithm we proposed in [20]. To summarize our previous work, the mask surface is first discretized into many small patches, such that the entire mask geometry is known if the mask thickness in each patch is known (we refer to a patch as a 'channel'). We then discretize the mask thickness levels in each channel, and the optimization problem becomes a selection problem. That is, we want to select one thickness level per channel while minimizing the MSE (4). Consequently, if we have S channels, and each channel is divided into R thickness levels, we can re-arrange $\mathbf{w} \in \{0,1\}^{RS}$ into a matrix $\mathbf{W} \in \{0,1\}^{R \times S}$. The matrix $\mathbf{W}$ is hence a selection matrix and should only have one non-zero element per column. To find a good mask, we want to select one such virtual sensor (or mask thickness level) per channel. In our previous works [11], [12], [20] we show that the final measurement matrix then becomes a summation of matrices:

$$\mathbf{A}(\mathbf{v}, \mathbf{w}) = \sum_{r=1}^{R} \sum_{s=1}^{S} [\mathbf{W}]_{r,s} \mathbf{A}_{r,s}(\mathbf{v}) \tag{6}$$

where each column of $\mathbf{W}$ has only one non-zero component, corresponding to the mask thickness of that channel. Equation (6) is how we parameterize $\mathbf{A}(\mathbf{v}, \mathbf{w})$ with respect to the mask shape.

Using a slight abuse of notation, the greedy algorithm is shown in Alg. 2. We use $\mathbf{w}_s$ to denote column s of matrix $\mathbf{W}$, and we use $\min_{\mathbf{w}_s} \text{MSE}(\mathbf{w}_s)$ to indicate that we minimize over column s of $\mathbf{W}$ only, keeping the other columns fixed. In Alg. 2, line 5-7 is used to pre-compute the MSE decrease per channel, and lines 8-9 then select a single channel to change the mask thickness (the channel that most decreases the MSE).

Algorithm 2 Greedy mask optimization algorithm

1: Input: starting mask $\mathbf{W}_0$
2: Output: optimized mask $\hat{\mathbf{W}}$
3: Initialize: $\hat{\mathbf{W}} = \mathbf{W}_0$
4: **do**
5: $\quad$ **for** $s = 1, 2, \ldots, S$ **do**
6: $\quad\quad e(s) = \min_{\|\mathbf{w}_s\|_0 = 1} \text{MSE}(\mathbf{w}_s)$
7: $\quad$ **end for**
8: $\quad \hat{s} = \arg\min_s e(s)$
9: $\quad \hat{\mathbf{w}}_{\hat{s}} = \arg\min_{\|\mathbf{w}_{\hat{s}}\|_0 = 1} \text{MSE}(\mathbf{w}_{\hat{s}})$
10: **until** local minimum is reached

C. Joint optimization

Finally, to jointly optimize for both parameters, we will alternate between optimizing only one of them, and keeping the other parameter fixed. As an initial mask, we take a completely flat mask. As an initial set of sensors, we take $3K$ randomly selected scanning positions. The algorithm will then optimize for the mask for these $3K$ positions, followed by selecting K positions out of all candidates, followed by re-

optimizing the mask, and so on and so forth. We summarize the procedure in Alg. 3.

We alternate between these two since both Alg. 1 and 2 are sub-optimal. If we, for example, fix the positions and optimize the mask, we may not find the *best* mask for this set of positions. Consequently, the optimal set of positions for this optimized mask may be different from the current set, and it is still possible to further optimize by running Alg. 1. The same can be said if we fixed the mask and optimize for positions. Hence, we alternate between the two algorithms multiple times until convergence, and the final result of Alg. 3 is not guaranteed to reach the global optimum.

Algorithm 3 Greedy sensor selection algorithm

1: Input: initial mask $\mathbf{w}_0$, initial positions $\hat{\mathbf{v}}_0$
2: Output: $\hat{\mathbf{v}}$, $\hat{\mathbf{w}}$
3: **do**
4: $\quad\hat{\mathbf{w}} \leftarrow$ output of Alg. 2, keeping $\hat{\mathbf{v}}$ fixed.
5: $\quad\hat{\mathbf{v}} \leftarrow$ output of Alg. 1, keeping $\hat{\mathbf{w}}$ fixed.
6: **until** local minimum is reached

III. Results

To verify the performance of our algorithm, we compare the joint design to 1) optimizing only the mask with fixed random scan positions, 2) optimizing only the scan positions with a fixed random mask, 3) randomly choosing both the mask and the sensing positions.

We use the following parameters. We assume the imaging medium consists of water with a speed of sound of 1491 m/s, and a plastic mask with a speed of sound of 2730 m/s. Hence the center wavelength in the imaging medium is $\lambda_0 = 372$ μm. The excitation pulse is a Gaussian-window modulated cosine with 4MHz center frequency. The mask is discretized into a circular shape of 437 channels on a Cartesian grid, and has a 3mm diameter, thereby sampling the mask at 2.8 channels per λ_0. The maximum mask thickness is 0.45 mm, whose range we discretize into 8 levels (5.7 levels per λ_0), to ensure that the mask has enough resolution to let the optimization algorithm create any possible pressure field. The imaging pixels are located within this area, at a depth of 6 mm, with dimensions of 11x11 mm (9x9 pixels). We use a 15x15 Cartesian grid of candidate scanning positions in a 14x14 mm area, parallel to the imaging plane, of which we want to select 11 scanning positions, resulting in a very high spatial undersampling (at best 11 samples for 11 mm in one spatial dimension, or 1 sample per $3\lambda_0$). During optimization, we choose a noise energy σ_n^2 such that the average SNR for a random mask with random sensing positions is around 10 dB.

Figure 1 shows the resulting mask shapes after optimization for all design strategies, and the sensing positions after optimization are shown in Fig. 2. The random masks are completely randomly drawn from a uniform distribution. A very clear structure is seen in the optimized masks, which shows a clustering, and many channels with the maximum mask thickness. The somewhat binary pattern of the mask may be due to the relatively low maximum mask thickness, (less than $2\lambda_0$). The mask may thus be a thresholded version of the optimal mask with a larger maximum mask thickness range.

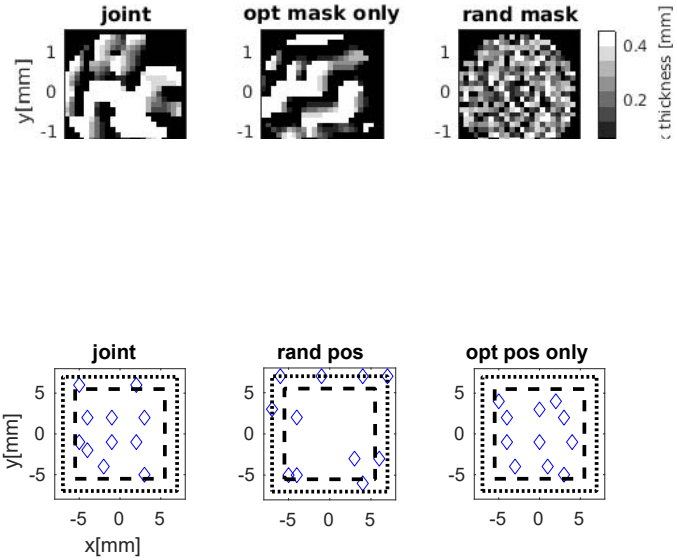

Fig. 2: Resulting sensing positions for various design strategies. The outer box indicates the region of candidate scanning positions. The inner box indicates the pixel ROI.

The optimal mask should be such that the received pulse-echo signals from overlapping beams of different scan positions are uncorrelated. Consequently, the mask should transmit different ultrasound fields to each direction, resulting in a non-symmetric mask. In other words, the spatial pressure field caused by the mask should have as much variation as possible. We plot the pressure fields for the center frequency $f_0 = 4$ MHz, as well as its spatial frequency spectrum in Fig. 3. The optimized mask is able to spread energy in space, creating overlap between different sensing positions, while also creating a highly varying pressure field. The random mask in this example is not able to create these high variations, resulting in poor imaging performance.

In Fig. 4, we show some example reconstructions for a test image shaped like a letter R, under an SNR of 10 dB, making sure that the variance of the test image is equal to one. In Fig. 5 we show the MSE (4) for varying SNR using the optimized setups at 10 dB. From these figures, we see that the jointly optimized setup greatly outperforms the other design strategies. Another observation is that the setup where only the mask is optimized has relatively good performance, suggesting that optimizing the mask is more important than finding good positions.

IV. Conclusion

We proposed an optimization scheme that alternatingly optimizes between the mask geometry and the sensor scan positions, keeping the other fixed. For either optimization step, we use a greedy optimization algorithm. We compared the imaging MSE for a 2D target image, and showed the superiority of the jointly optimized setup compared to a completely

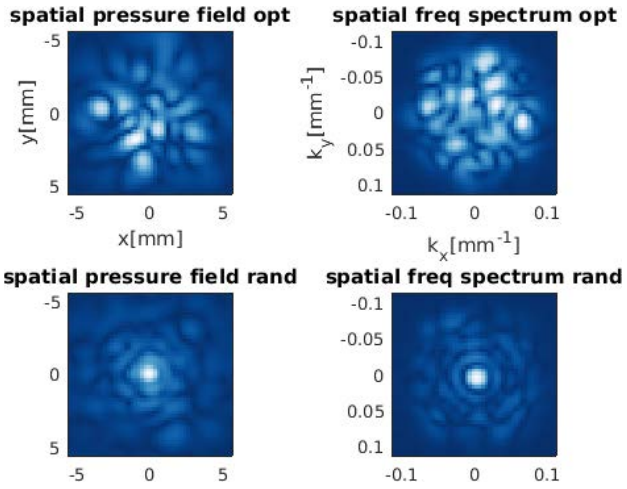

Fig. 3: Top: spatial normalized pressure distributions for the jointly optimized mask, and a realization of a random mask. Bottom: their respective spatial frequency spectra.

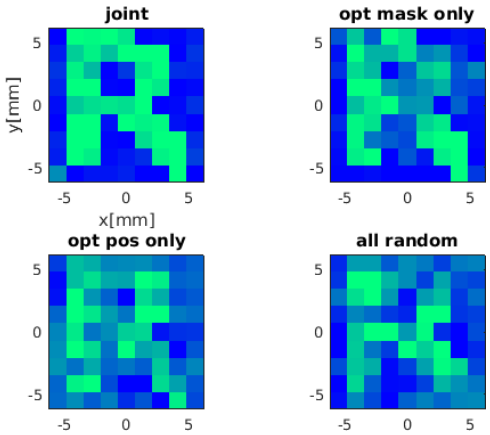

Fig. 4: Example reconstruction for a letter-shaped target image.

random design strategy. Moreover, we compared our design to two alternative designs. In the first setup the positions are random, and only the mask is optimized. In the second, the mask shape is random, and only the scanning positions are optimized. By analyzing the spatial wavefields, we observed that a good mask creates a highly varying pressure field in space. Our results show that optimizing for the mask is more important than finding good scan positions, although the joint design outperforms all other setups.

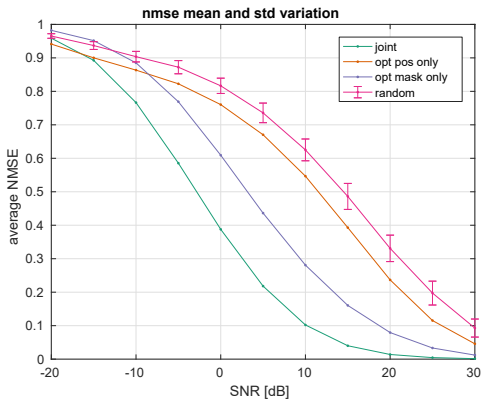

Fig. 5: Imaging MSE for various SNR scenarios. The mask and sensing positions were originally optimized for an SNR of around 10 dB. The vertical bars indicate the MSE standard deviation over 100 setups where both position and mask shape is randomized.

References

[1] D. L. Donoho, "Compressed sensing," *IEEE Transactions on information theory*, vol. 52, no. 4, pp. 1289–1306, 2006.

[2] E. J. Candès, J. Romberg, and T. Tao, "Robust uncertainty principles: Exact signal reconstruction from highly incomplete frequency information," *IEEE Transactions on information theory*, vol. 52, no. 2, pp. 489–509, 2006.

[3] E. J. Candes and T. Tao, "Near-optimal signal recovery from random projections: Universal encoding strategies?" *IEEE transactions on information theory*, vol. 52, no. 12, pp. 5406–5425, 2006.

[4] E. J. Candès and M. B. Wakin, "An introduction to compressive sampling," *IEEE signal processing magazine*, vol. 25, no. 2, pp. 21–30, 2008.

[5] H. Liebgott, R. Prost, and D. Friboulet, "Pre-beamformed rf signal reconstruction in medical ultrasound using compressive sensing," *Ultrasonics*, vol. 53, no. 2, pp. 525–533, 2013.

[6] C. Quinsac, A. Basarab, and D. Kouamé, "Frequency domain compressive sampling for ultrasound imaging," *Advances in Acoustics and Vibration*, vol. 2012, 2012.

[7] T. Chernyakova and Y. Eldar, "Fourier-domain beamforming: the path to compressed ultrasound imaging," *IEEE transactions on ultrasonics, ferroelectrics, and frequency control*, vol. 61, no. 8, pp. 1252–1267, 2014.

[8] M. F. Schiffner and G. Schmitz, "Fast pulse-echo ultrasound imaging employing compressive sensing," in *Ultrasonics Symposium (IUS), 2011 IEEE International*. IEEE, 2011, pp. 688–691.

[9] G. David, J.-l. Robert, B. Zhang, and A. F. Laine, "Time domain compressive beam forming of ultrasound signals," *The Journal of the Acoustical Society of America*, vol. 137, no. 5, pp. 2773–2784, 2015.

[10] A. Besson, R. E. Carrillo, O. Bernard, Y. Wiaux, and J.-P. Thiran, "Compressed delay-and-sum beamforming for ultrafast ultrasound imaging," in *Image Processing (ICIP), 2016 IEEE International Conference on*. Ieee, 2016, pp. 2509–2513.

[11] P. Kruizinga, P. van der Meulen, A. Fedjajevs, F. Mastik, G. Springeling, N. de Jong, J. G. Bosch, and G. Leus, "Compressive 3d ultrasound imaging using a single sensor," *Science advances*, vol. 3, no. 12, 2017.

[12] J. Janjic, P. Kruizinga, P. van der Meulen, G. Springeling, F. Mastik, G. Leus, J. G. Bosch, A. F. van der Steen, and G. van Soest, "Structured ultrasound microscopy," *Applied Physics Letters*, vol. 112, no. 25, p. 251901, 2018.

[13] S. Joshi and S. Boyd, "Sensor selection via convex optimization," *IEEE Transactions on Signal Processing*, vol. 57, no. 2, pp. 451–462, 2009.

[14] S. P. Chepuri and G. Leus, "Sparsity-promoting sensor selection for non-linear measurement models." *IEEE Trans. Signal Processing*, vol. 63, no. 3, pp. 684–698, 2015.

[15] F. Bian, D. Kempe, and R. Govindan, "Utility based sensor selection," in *Proceedings of the 5th international conference on Information processing in sensor networks*. ACM, 2006, pp. 11–18.

[16] A. Krause and C. Guestrin, "Near-optimal observation selection using submodular functions," in *AAAI*, vol. 7, 2007, pp. 1650–1654.

[17] M. Coutino, S. Chepuri, and G. Leus, "Near-optimal greedy sensor selection for mvdr beamforming with modular budget constraint," in *Signal Processing Conference (EUSIPCO), 2017 25th European*. IEEE, 2017, pp. 1981–1985.

[18] G. L. Nemhauser, L. A. Wolsey, and M. L. Fisher, "An analysis of approximations for maximizing submodular set functionsi," *Mathematical programming*, vol. 14, no. 1, pp. 265–294, 1978.

[19] L. Chamon and A. Ribeiro, "Approximate supermodularity bounds for experimental design," in *Advances in Neural Information Processing Systems*, 2017, pp. 5403–5412.

[20] P. van der Meulen, P. Kruizinga, J. G. Bosch, and G. Leus, "Spatial compression in ultrasound imaging," in *Signals, Systems, and Computers, 2017 51st Asilomar Conference on*. IEEE, 2017, pp. 1016–1020.